Electronic Supplementary Material (ESI) for RSC Advances.

Aqueous Colloidal Systems of Bovine Serum Albumin and Functionalized Surface Active Ionic Liquids for Material Transport

Gagandeep Singh, Manvir Kaur, Vinod Kumar Aswal,[b] Tejwant Singh Kang*,[a]

[a]*Department of Chemistry, UGC-Centre for Advance Studies – II, Guru Nanak Dev University, Amritsar, 143005, India.*

[b]*Solid State Physics Division, Bhabha Atomic Research Centre, Mumbai 400085, India*

Supporting Information

**To whom correspondence should be addressed:*

e-mail: tejwantsinghkang@gmail.com; tejwant.tej@gmail.comTel: +91-183-2258802-Ext-3207

Annexure S1.

S1.1. Materials: Bovine Serum Albumin (BSA) lyophilized powder; ≥96% (agarose gel electrophoresis), Rhodamine 6G (dye content 99 %) were procured from Sigma Aldrich and used without any modification. The SAILs under investigation i.e 1-dodecyl-3-methyl imidazolium chloride [C_{12}mim][Cl] and its ester and amide counterparts [C_{12}Amim][Cl] and [C_{12}Emim][Cl] have been used from the same lot as that reported in our earlier report. To ensure their chemical suitability all the preserved SAILs were again characterized by NMR before use. Further the SAILs were degassed and dried under vacuum for 2 days at 70^{o}C to remove moisture contents before any measurement. The samples of SAILs and BSA were weighed on analytical balance having precision of 0.0001g (Precisa) and were dissolved in degassed Millipore water for preparing their stock solutions. Pyrene as a molecular probe for extrinsic fluorescence measurements was purchased from Sigma Aldrich (99%) and used after re-crystallization from ethanol.

S1.2. Methods: In all experiment, titration method was used to investigate the physicochemical behavior of colloidal systems at 298.15K. In each case the titration of BSA (0.1%) is performed with the concentrated SAILs solution which is generally made 10-15 times higher than their respective SAIL critical micelle concentration (*cmc*) depending upon the critical volume of sample (0.1% BSA) needed in the titration vessel.

S1.2.1. Tensiometry: Interfacial behavior of colloidal systems of BSA and SAILs under investigation has been explored using KRÜSS (Hamburg, Germany) Easy Dyne tensiometer by ring method using a platinum ring. The measurements were performed by adding the concentrated stock solution of respective SAILs to an aqueous solution of BSA and stirred for 2-3 min and equilibrated for 4 min. The temperature during experiment was monitored and controlled using a Julabo water thermostat within ±0.1 K. Measurements were performed in triplicate with an uncertainty of ± 0.15 mN m^{-1}.

S1.2.2. Conductometry: Digital conductivity meter (Systronics 308) having cell of unit cell constant has been used for measuring specific conductance (κ) of SAIL solutions in presence and absence of BSA. The temperature of measurement cell was controlled with a water thermostat within ± 0.1 K. Measurements were performed in triplicate with an uncertainty of less than 1%.

S1.2.3. Turbidimetry: Turbidity measurements were performed on Turbidity Meter from Cole-Parmer (Oakton T-100 Handheld). Instrument provides turbidity of system under investigation in terms of nephelometric turbidity units (NTU) which is deduced using infrared LED light source with accuracy of 0.01 NTU.

S1.2.4. Steady-state fluorescence: Steady-state fluorescence measurements were performed using a Perkin Elmer LS-55 spectrophotometer using a quartz cuvette of path length 1 cm. The variation in the microenvironment associated with SAIL-BSA aggregates as the function of SAIL concentration has been explored using polarity sensitive pyrene probe. The I_1/I_3 ratio of pyrene in SAILs solution in the presence and absence of BSA reveals the alternations occurring during the complexation process due to high sensitivity of emission intensity of vibronic peaks of first (I_1 at 373 nm) to third vibronic peak (I_3 at 384 nm) pyrene.[1] Fluorescence emission spectra were recorded in wavelength range 350–550 nm at an excitation wavelength of 334 nm by keeping the excitation and emission slit widths of 4nm, each. The concentration of pyrene was maintained at 2 μM to avoid excimer formation.

S1.2.5. Isothermal Titration Calorimetry (ITC): Thermodynamic parameters during the complexation between SAILs and BSA systems were calculated using isothermal titration calorimeter (MicroCal ITC200, USA). The sample cell and reference cell of ITC was loaded with 200μl solution of BSA (0.1% BSA solution in 5mM phosphate buffer) and phosphate buffer respectively from same stock in all experiments. The stock solution of SAILs were injected in the sample vessel in 20 injections of 2 μL each using Hamilton syringe. The sample cell was stirred continuous fixed speed of 500 rpm to ensure the complete mixing of solution contents followed by an interval time of 120s between successive injections for thermal equilibration.

S1.2.6. Docking Studies: AutoDock Vina software is used for docking simulations to find the possible binding site location and the relative affinity of the investigated SAILs on BSA. Further, same software was used for finding the possible binding sites of SAIL-BSA complex with R6G dye. The program is embedded with the Lamarckian Genetic Algorithm (LGA) for the analysis of best binding conformation of ligand-protein geometry and efficiently dock the desired ligand into proteins without the prior knowledge of binding site.[2,3] The native crystal structure of BSA containing the exact information of atomic coordinates present in protein was taken from Protein Data Bank with PDB ID: 4F5S. The obtained protein structure is then reconstructed and made

refined in AutoDock Tools by removing the solvent water molecules followed by the addition of hydrogen atoms. The three-dimensional structure of the investigated SAILs is prepared in Gaussian 09 software and is optimized at DFT//B3LYP/6-31G (d,p) level of theory. Blind Docking was carried out by setting the configuration of grid size to 82, 68, 84 along x, y, z-axes with a grid spacing 1Å. The grid centre was made 67.668 Å, 26.361 Å and 89.74 Å along x, y and z-axis respectively. The exhaustiveness or search space is set 2000 to find the most stable SAIL-BSA conformation. To check the reproducibility of calculated results, the search algorithm which uses a unique random seed is performed three times for each SAIL-BSA system. Out of nine different conformations results, the docked conformation of SAIL-BSA having minimum energy was selected. The docked conformations were visualized using PyMOL 2.0.6 software package.

S1.2.7. Zeta-potential Measurements: Zeta-potential (ζ-potential) measurements of SAIL-BSA and Rhodamine 6G system under investigation has been performed on Zetasizer NanoZS (Malvern, instruments, UK) equipped with a He-Ne laser (632.8 nm, 4mW). The system has an inbuilt temperature controller with an accuracy ±0.1 K at a scattering angle of 173° to the incident beam. Prior to measurements, all the solutions were filtered by membrane filter having pore size of 0.45μm to eliminate the chance of any contamination by dust particles.

S1.2.8. Confocal Laser Scanning Microscopy: Confocal laser scanning microscopy (CLSM) was performed using a Carl Zeiss LSM 510 confocal microscope. A drop of solution of BSA having respective SAIL-2 and R6G at desired concentration was placed on glass bottomed dishes (Matsunami Glass Ind., Ltd.).

S1.2.9. Small Angle Neutron Scattering (SANS) Measurements: SANS measurements has been carried out using SANS diffractometer operating at Dhruva reactor located at Bhabha Atomic Research Centre (BARC), Mumbai, India. During experiment a beam of neutron having wavelength (λ) 5.2 Å and resolution (Δλ/λ) ≈15% was incident on sample. Further the scattered beam of neutrons was detected in an angular range of 0.5-15° using a linear position-sensitive detector (PSD). The samples to be analyzed are kept in a quartz sample holder having a thickness of 0.5 cm maintained at constant temperature at 30 ± 0.1 °C during measurements. The wave-vector transfer, Q ($Q = 4\pi \sin(\theta/2)/\lambda$ has been determined from scattered neutrons, where θ is the scattering angle) in the range of 0.015-0.3 $Å^{-1}$. The collected SANS data was corrected for

various contributing factors such as background, empty cell contribution and transmission and was presented on an absolute scale using standard protocols. All the samples were prepared in D_2O in order to minimize incoherent scattering and to increase the contrast.

Annexure S2:

1. Γ_{max}, Gibbs surface excess is calculated using Gibbs adsorption equation which is given as follow:

$$\Gamma_{max} = -\frac{1}{2.303nRT}\left(\frac{d\gamma}{d\log C}\right)_T$$

here n is the number of ions formed per unit molecule of surface active ionic liquid surfactant (SAILs) in solution upon dissolution which is 2 for all the SAILs under investigation in the present study, T is absolute temperature, R is universal gas constant and [C] is molar concentration of SAILs in solution.

2. A_{min} minimum area per molecule at the air–solution interface is calculated from relation:

$$A_{min}=10^{20}/N_A\Gamma_{max}$$

where N_A is Avogadro's number.

3. ΔG^o_{ads} standard free energy of adsorption of surfactant is obtained from equation:

$$\Delta G^o_{ads} = \Delta G^o_{mic} - \frac{\pi_{cmc}}{\Gamma max}$$

where π_{cmc} (critical micelle concentration, cmc)is surface pressure of solution at saturated air-solution interface and is calculated as:

$$\pi_{cmc} = \gamma_o - \gamma_{cmc}$$

where γ_0 is the surface tension of aqueous solution with and without BSA and γ_{cmc} is the surface tension of solution of SAILs at cmc point with and without BSA respectively.[4,5]

4. ΔG^o_m standard free energy of micellization of SAILs in solution at their cmc point is calculated using equation:

$$G^o_m=(1+\beta)RT\ \ln X_{cmc}$$

where R is universal gas constant, T is absolute temperature, X_{cmc} is cmc in mole fraction and β is degree of counter-ion binding, which is calculated from the ratio of slopes ($1\text{-}S_2/S_1$) where $S_1$and S_2 are the slopes of pre and post micellar region respectively (i.e. before and after the cmc point) of κ vs C plots of different SAILs in the absence and presence of BSA.

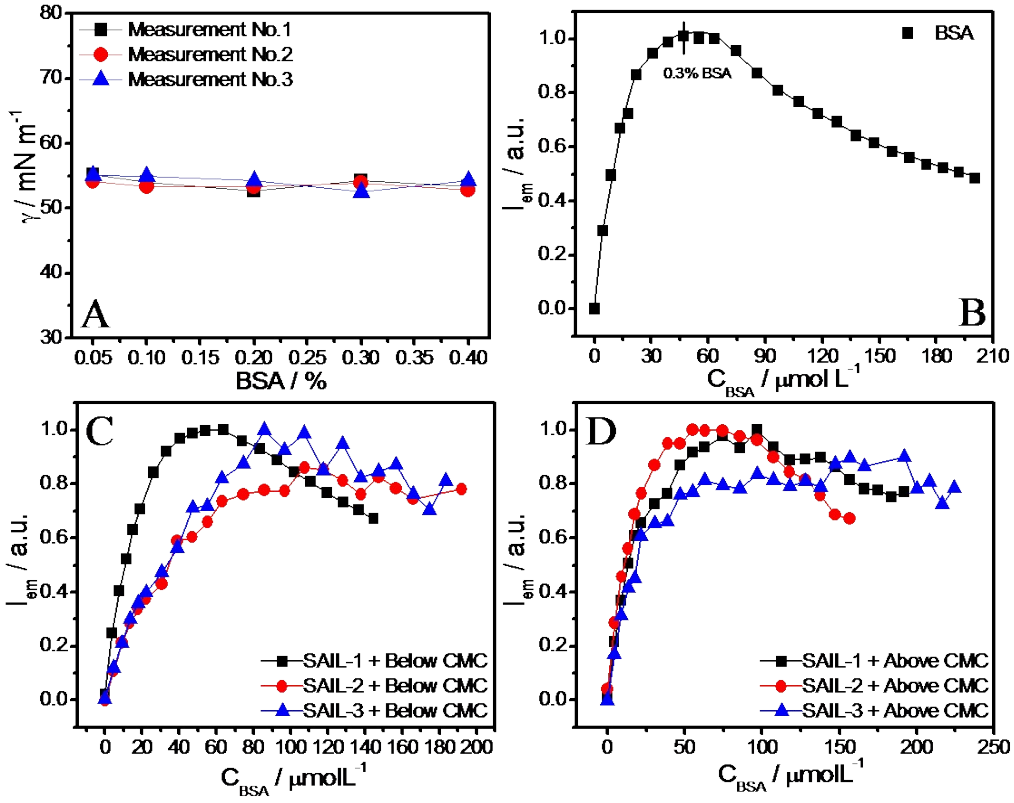

Fig. S1(A–D), (A) surface tension profile, (B) I_{flr} of BSA, and (C, D) I_{flr} of BSA in presence of SAILs below and above their respective cmc, respectively as a function of concentration of BSA. Figure S1A shows the surface tension profile of BSA at its different concentration at air-solution interface. On the other hand Figure S1B shows the variations in the emission intensity of intrinsic fluorescence (I_{em}) of BSA. The I_{em} profile of BSA increases up to maximum at 0.3% (wt/wt) and then begins to decrease afterwards indicating the quenching of fluorophore intensity of BSA caused by the inter-molecular interaction between BSA molecules which presumably resulted by the conformational changes in BSA. Therefore, in the present study we have chosen 0.1% concentration of BSA in order to avoid any sort of inter-molecular interactions between BSA molecules, which could affect its interactions with SAILs. Similar inferences have been

gained from fluorescence measurements made by fixing the SAIL concentration (below and above *cmc*) and by varying the concentration of BSA.

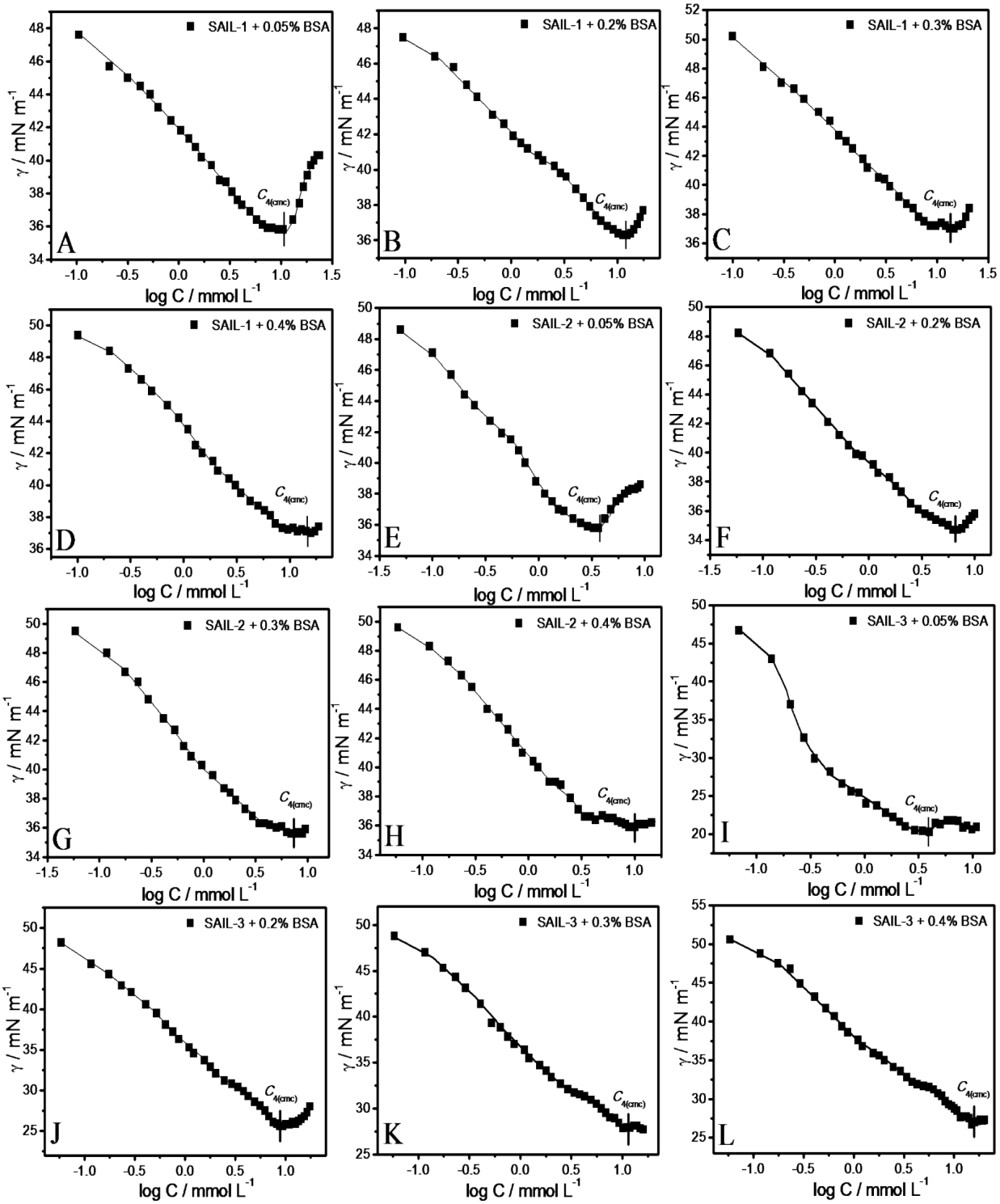

Fig. S2 (A–L). The plots of surface tension at fixed concentration of BSA (0.05%, 0.2%, 0.3% and 0.4%) with SAIL-1, SAIL-2 and SAIL-3.

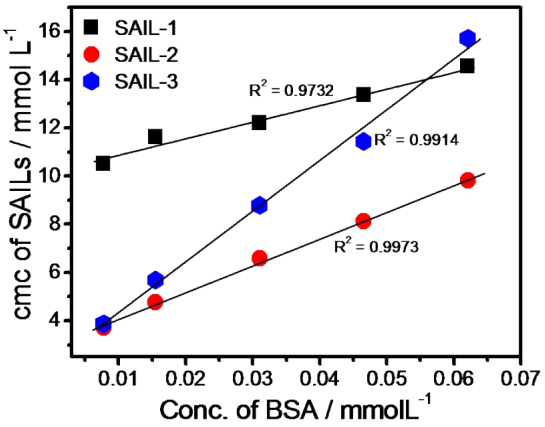

Fig. S3. Variaiton of *cmc's* of SAILs against concentration of BSA as obtained from surface tension measurements (Fig. S2). The number of SAIL units bound to BSA at cmc of respective SAILs are obtained by linear fitting using equation:[6]

$[S]_{cmc} = [S]_{free} + N \times [P]$

where $[S]_{cmc}$ is concentration of SAIL at cmc, $[S]_{free}$ is concentration of free SAIL, [P] refers to the concentration of protein under investigation, and N is the number of SAIL units bound to BSA.

Fig. S4. TEM images of SAIL-1, SAIL-2 and SAIL-3 at their respective critical micelle concentration (*cmc*) showing spherical (in diameter) shape in aqueous buffer solution.

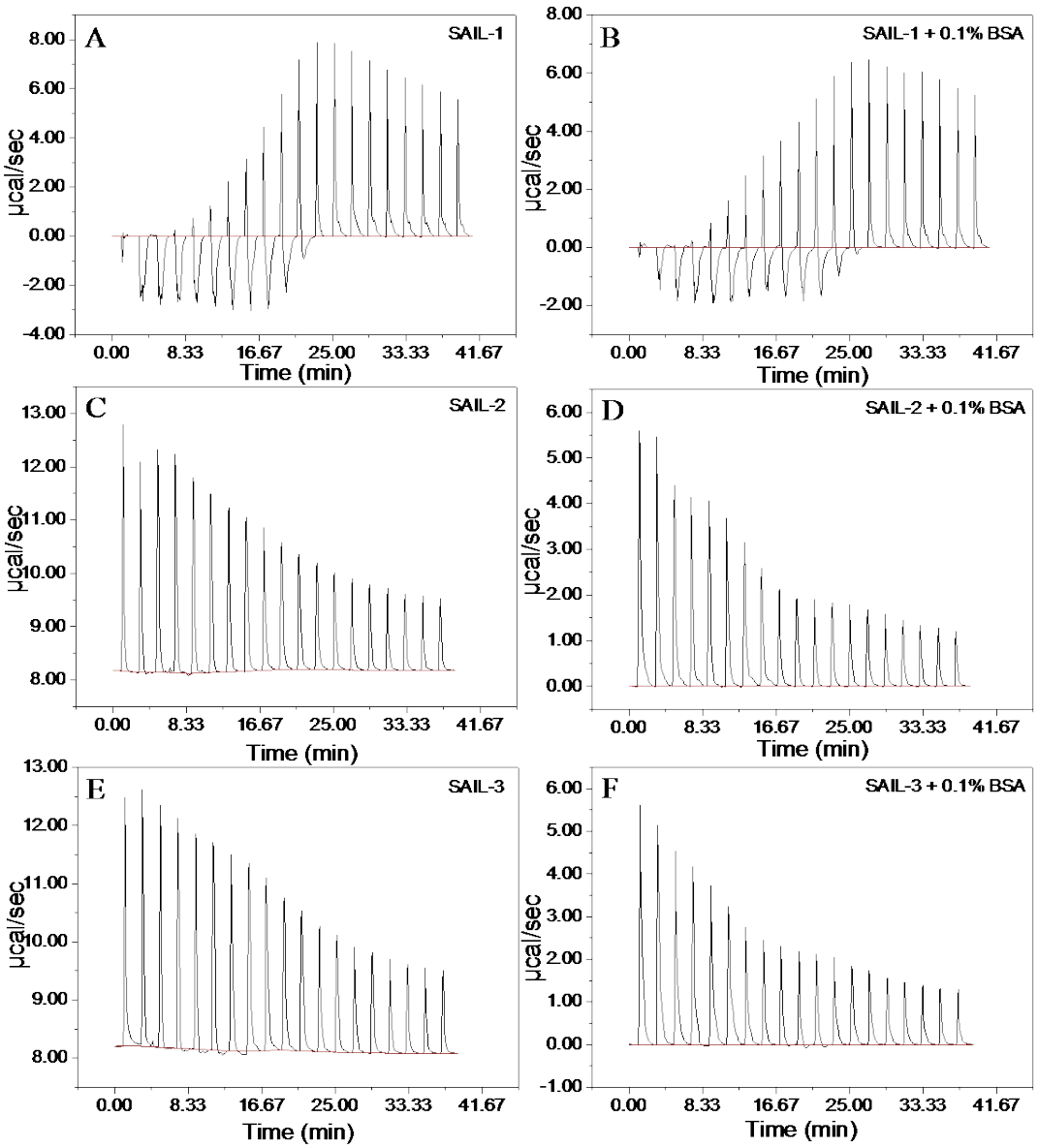

Fig. S5 (A-F). Differential power plots of aqueous buffer solution of SAILs in the presence and absence of BSA at 298.15K. In case of SAIL-1, the shape of obtained enthalpogram (Fig. S5A, SI) in the absence and presence of BSA is quite similar, which is suggestive of rather weaker interactions prevailing in components of colloidal system. On the other hand, the shape and nature of enthalpograms in case of SAIL-2 and SAIL-3 are quite different in the absence and presence of BSA (Fig. S5B and C, SI), till $C_{4(cmc)}$. However, beyond $C_{4(cmc)}$, the obtained enthalpograms in colloidal systems overlaps with that obtained for aqueous SAIL systems. This indicates that the thermodynamic behavior of complexation of SAIL-2 and SAIL-3 with BSA in dilute concentration regime of SAILs is dominated by different forces of interactions, whereas the formation of micelles, after $C_{4(cmc)}$, dominates the thermodynamic behavior.

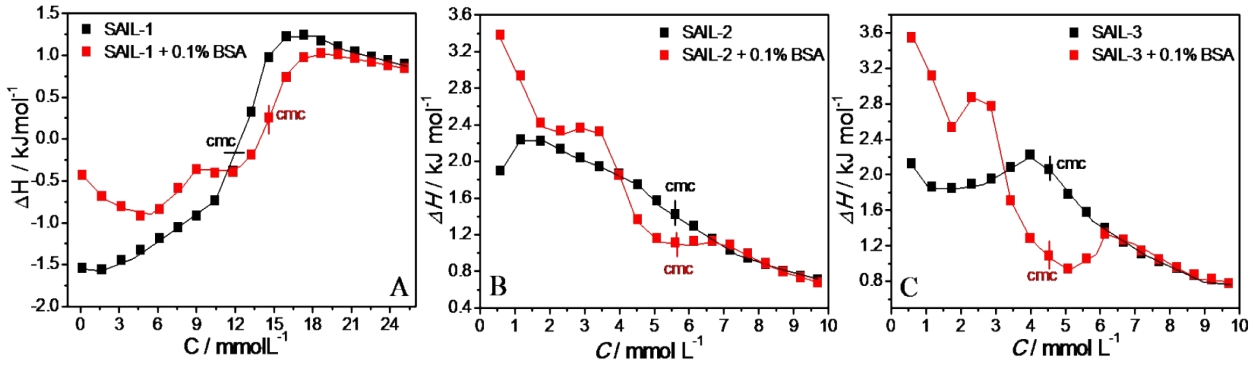

Fig. S6 (A-C). Enthalpogram of SAILs in aqueous buffer solution with and without BSA as a function of concentration of different SAILs at 273.15K.

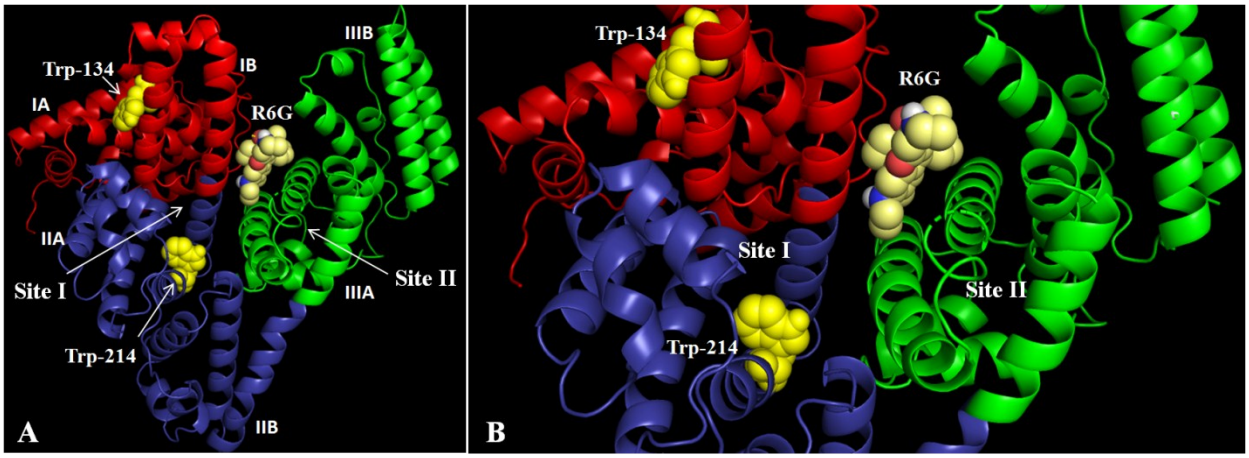

Fig. S7 (A,B). (A) Docked conformation of R6G in the centre between three domains of BSA along with the location of Trp residues and binding site locations in subdomain IIA and IIIA (B) Enlarged view.

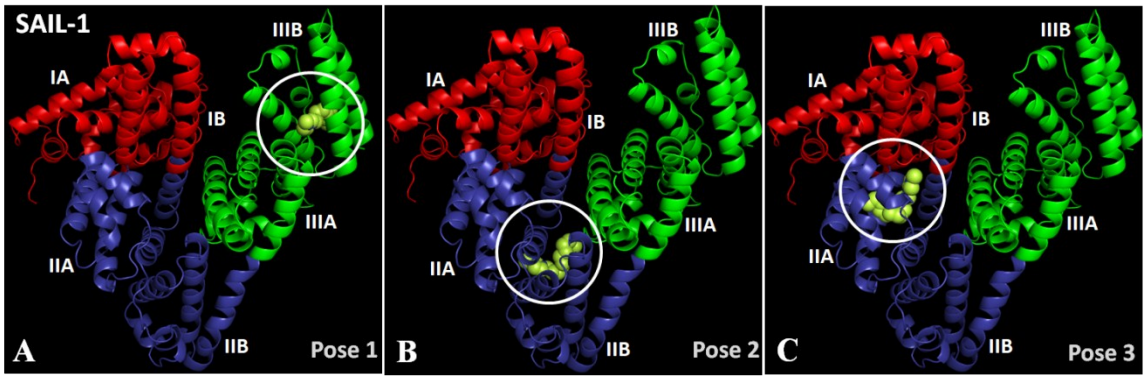

Fig. S8(A-C). Docked conformation of SAIL-1-BSA system showing the high affinity binding sites for SAIL-1 on BSA in different poses.

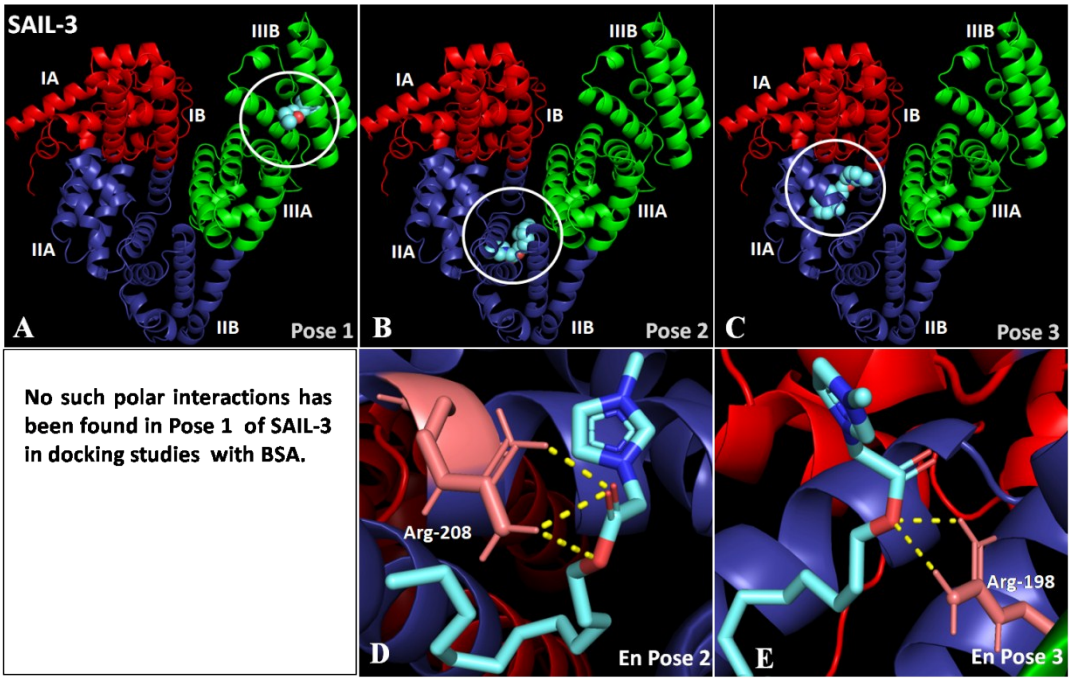

Fig. S9 (A-E). (A-C) Docked conformation of SAIL-3-BSA system showing the high affinity binding sites for SAIL-3 on BSA in different poses; (D,E) Enlarged view of respective poses.

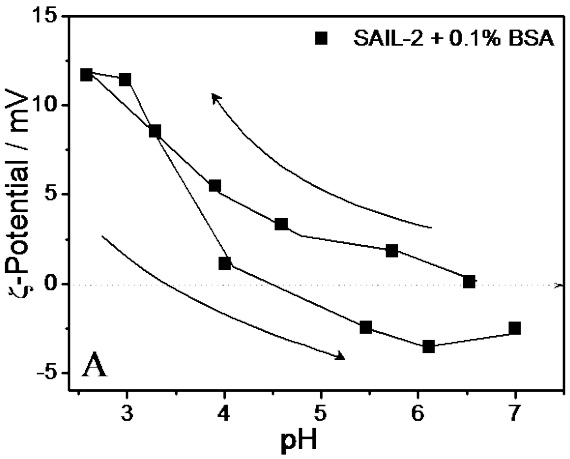

Fig. S10: Zeta potential measurements on SAIL-2-BSA system at variable pH at 298.15K.

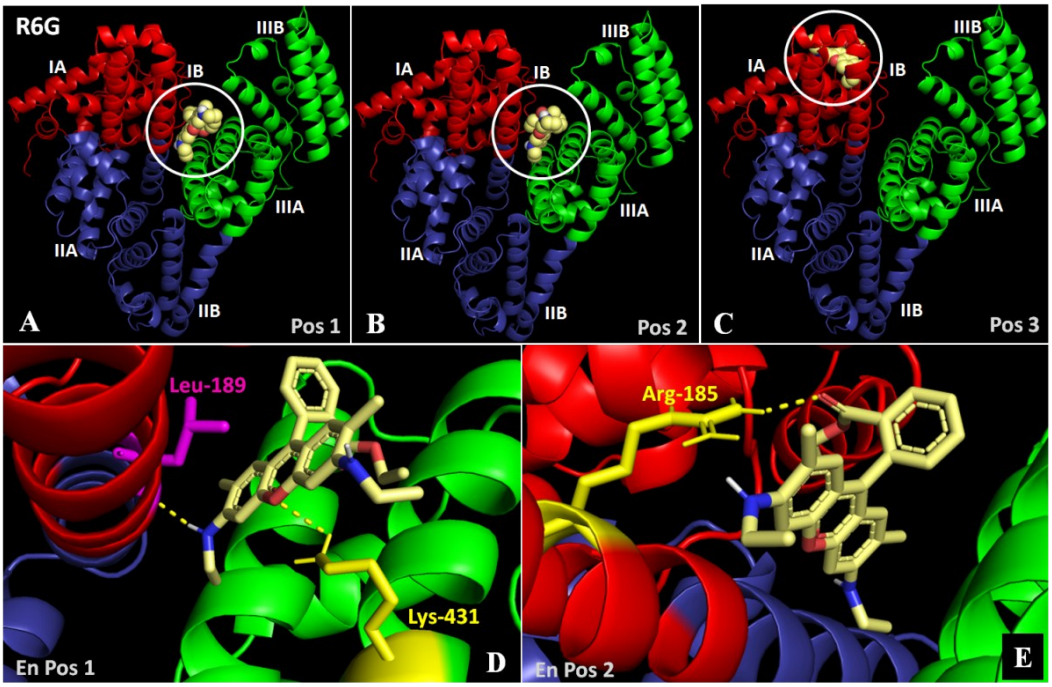

Fig. S11 (A-E). Docked conformation of R6G-BSA system showing the high affinity binding sites for R6G on BSA in different poses; (D,E) Enlarged view of respective poses. The careful analysis of docking results reveals nine best R6G-BSA conformations (Table S5) to have only two distinct binding site locations, one at the centre of three domains (Fig. S7 (A,B), SI) and another at domain I (Fig. S7C, SI). R6G is found to bind in a cavity between three domains interacting mainly with domain I and domain III.

The analysis of docking results reveals nine best R6G-BSA conformations to have only two distinct binding site locations, one at the centre of three domains (Fig. S7A,B) and another at domain I (Fig. S7C). In pose 1 (Fig. S7A, D), R6G is interacting via polar interactions, one through its NH group with oxygen atom of carbonyl group of -COOH of Leu-189 (pink) which is present in domain I (Fig. S7A,D) and another with oxygen atom of hetrocyclic ring with NH_2 of Lys-431 (yellow) present in domain II (Fig. S7A, D). Similarly in pose 2 (Fig. S7B, E), R6G makes polar link through oxygen atom of carbonyl group with NH_2 group of Arg-185 (yellow) present in domain I (Fig. S7E). But this cavity i.e. binding site of R6G fades away with decrease in pH due to the opening of BSA structure, however the binding location at domain I remain unaffected even at low pH. Results obtained by docking R6B with BSA reveals that due to greater hydrophilicity, larger molecular size and spatial geometry R6B got fitted in none of the earlier proposed sites on BSA but however occupies the central position of BSA between IB and IIA (Fig. S4). Repeated docking simulations on R6B with BSA gave same results along with same free energy of binding affinity (32.6 kJ mol^{-1}) which is almost equal to the binding affinity of SAILs binding on BSA.

Table S1: The value of critical micelle concentration (*cmc*) obtained from tensiometry at different concentrations of BSA along with parameters obtained by model fitting at 298.15 K in phosphate buffer at pH 7.4.

S.No.	Concentration of BSA	*cmc* of different SAILs (in mM)		
		SAIL-1	SAIL-2	SAIL-3
1.	0.05%	10.51	3.72	3.88
2.	0.1%	11.62	4.76	5.69
3.	0.2%	12.21	6.59	8.79
4.	0.3%	13.37	8.12	11.44
5.	0.4%	14.56	9.82	15.72
	SAIL units bound to BSA	69.7	110.9	210.7

Table S2: The critical micelle concentration (cmc) values of different SAILs obtained from various techniques.

SAILs	ST	Cond.	I_1/I_3	Flr.230	Flr. (λ_{max})	ITC	Turb.
In aqueous buffer solution							
SAIL-1	13.09	13.01	8.42	-	-	11.97	-
SAIL-2	2.07	4.89	3.91	-	-	5.69	-
SAIL-3	2.34	4.92	2.67	-	-	4.59	-
In presence of 0.1% BSA in buffer solution							
SAIL-1	11.62	9.46	3.34	10.39	11.81	14.56	9.09
SAIL-2	4.76	6.52	2.95	5.33	5.76	6.86	2.86
SAIL-3	5.69	5.72	2.89	4.81	5.18	6.55	2.62

Table S3: The interfacial parameter and thermodynamic data obtained from tensiometric and conductivity profiles of SAILs with and without BSA.

SAILs	γ_{cmc}	π_{cmc}	Γ_{max} $\times 10^6$	A_{min}	ΔG_{ads}^{o}	β	ΔG_{mic}^{o}
In aqueous buffer solution							
SAIL-1	30.5	40.4	1.94	85.41	-51.15	0.47	-30.37
SAIL-2	35.2	36.5	2.32	71.72	-53.86	0.65	-38.09
SAIL-3	20.7	51.0	3.57	46.55	-49.59	0.53	-35.29
In presence of 0.1% BSA in buffer solution							
SAIL-1	36.5	17.5	0.59	282.1	-57.04	0.27	-27.29
SAIL-2	35.6	17.9	0.62	267.3	-64.16	0.58	-35.34
SAIL-3	27.3	28.5	1.05	157.4	-60.49	0.47	-33.47

β is found to be decreased by 1.74, 1.12 and 1.12 times for SAIL-1, SAIL-2 and SAIL-3, respectively in presence of BSA. Depression in β values may be assigned to the presence of interactions between forming micelles and BSA at micelle-solution interface and the adsorption of BSA stabilizes the micelles of SAILs. This results in relatively lesser involvement of counter-ions in the formation of micelle.

Table S4 (A,B). (A) SANS analysis of 1% BSA + SAIL at C_1 of respective SAILs.

System	Structure (Oblate Ellipsoidal)	
	Semiminor axis (a)	Semimajor axis (b=c)
BSA + SAIL-1	15.0 Å	42.0 Å
BSA + SAIL-2		
BSA + SAIL-3		

(B) SANS analysis of 1% BSA + SAIL at higher SAIL concentrations

System	Structure (Bead-Necklace)		
	Micellar core radius	Number of micelles per cluster	Separation between the centre of two nearest micelles
BSA + SAIL-1	16.7 Å	7	43.8 Å
BSA + SAIL-2		4	40.2 Å
BSA + SAIL-3		5	39.4 Å

Table S5: Thermodynamics of the investigated SAIL systems has been divided into four regions such as C_i-C_2, C_2-C_3, C_3-C_4, C_4-C_s and their corresponding enthalpy changes has been provided. The values of enthalpy and the division of different regions were determined from difference plot presented in the manuscript. C_i is the concentration of first addition and C_s is the concentration of SAIL where ITC curve saturates.

SAILs	C_i-C_2 ($\Delta^{H_1^o}$)	C_2-C_3 ($\Delta^{H_2^o}$)	C_3-C_4 ($\Delta^{H_3^o}$)	C_4-C_s ($\Delta^{H_4^o}$)
SAIL-1	-0.46	-0.08	-1.28	+0.66
SAIL-2	-1.30	+0.19	-0.79	+0.44
SAIL-3	-0.73	+0.14	-1.79	+1.00

Table S6: Binding affinity of SAILs with BSA obtained from docking simulation in nine different conformations along with their root mean square deviation (rmsd) values of lower bound (l.b) and upper bound (u.b.) for each conformation.

Mode	SAIL-1 affinity ($kJ\ mol^{-1}$)	Distance from best mode		SAIL-2 affinity ($kJ\ mol^{-1}$)	Distance from best mode		SAIL-3 affinity ($kJ\ mol^{-1}$)	Distance from best mode	
		rmsd l.b.	rmsd u.b.		rmsd l.b.	rmsd u.b.		rmsd l.b.	rmsd u.b.
1	-30.9	0.000	0.000	-34.7	0.000	0.000	-31.7	0.000	0.000
2	-30.1	3.166	9.442	-34.7	0.074	5.099	-30.1	39.786	43.663
3	-29.7	1.189	1.75	-34.7	0.066	4.118	-29.7	41.944	44.203
4	-28.4	3.873	9.258	-34.3	35.587	38.156	-29.7	41.352	43.598
5	-28.0	2.806	9.701	-33.8	14.069	16.451	-29.7	4.316	11.191
6	-27.1	41.129	44.62	-33.4	14.055	16.503	-29.2	41.622	43.849
7	-27.1	41.272	44.77	-33.4	14.064	16.23	-29.2	41.712	43.904
8	-27.1	39.776	44.50	-33.4	14.119	16.191	-28.8	29.638	32.492
9	-26.7	40.733	44.14	-33.4	0.874	3.124	-28.8	1.967	3.479

Table S7: The binding affinity of Rhodamine with BSA obtained from docking simulation in nine different conformations along with their root mean square deviation (rmsd) values of lower bound (l.b) and upper bound (u.b.) for each conformation.

Mode	Rhodamine affinity (kJ mol^{-1})	Distance from best Mode	
		rmsd l.b.	rmsd u.b.
1	-32.6	0	0
2	-32.6	0.278	5.972
3	-32.2	1.967	3.04
4	-31.7	1.971	6.593
5	-30.9	4.476	6.577
6	-30.9	3.265	6.201
7	-30.1	4.465	8.716
8	-30.1	3.26	8.538
9	-29.7	16.367	19.375

References:

1. K. Kalyanasundaram and J. K. Thomas, *J. Am. Chem. Soc.*, 1977, **99,** 2039–2044.
2. O. Trott and A. J. Olson, *J. Comput. Chem.*, 2010, **31,** 455–461.
3. M. M. Jaghoori, B. Bleijlevens and S. D. Olabarriaga, *J. Comput. Aided Mol. Des*, 2016, **30,** 237–249.
4. M. J. Rosen, Surfactants and Interfacial Phenomena, 3rd ed.: Wiley-Interscience; Hoboken, NJ, 2004.
5. J. Eastoe, S. Nave, A. Downer, A. Paul, A. Rankin, K. Tribe and J. Penfold, *Langmuir*, 2000, **16,** 4511−4518.
6. D. Otzen, *Biochim. Biophys. Acta, Proteins Proteomics* 2011, **1814**, 562-591.